Investigating the Role of Wnt-Pathway Inhibition in Mouse Breast Cancer Tumor Growth and Metastasis

Thesis Submitted in Partial Fulfillment of the Requirements of the Jay and Jeanie Schottenstein Honors Program

Yeshiva College

Yeshiva University

January 2021

Justin Stein

Mentor: Dr. Sumanta Goswami

Department of Biology

Table of Contents

General Abstract

Aside from skin cancers, breast cancer is the most commonly diagnosed cancer in American woman with 300,000 Americans diagnosed each year. Although great strides have been made in treating breast cancer, there are few effective treatment options once it spreads to other parts of the body (metastatic breast cancer). Metastatic breast cancer comprises the vast majority of breast cancer related deaths and individuals with metastatic breast cancer have a 5-year survival rate of 27% (ASCO, 2019). Previous studies have shown that only a small population of breast cancer cells within the tumor are capable of spreading and these cells are known to be chemotherapy and drug resistant. Additionally, research has also indicated that targeting a specific receptor on these cells has the potential to eradicate these cells precisely. In this project, a prospective monoclonal antibody treatment that targets this receptor was investigated to see how well it reduces the growth of breast cancer tumors and prevents the spread of the disease. This prospective treatment has the potential to develop into a much-needed medication that could result in increased long-term survival of breast cancer patients.

Scientific Abstract

Metastatic breast cancer comprises the vast majority of breast cancer related deaths and individuals with metastatic breast cancer have a 5-year survival rate of 27% (ASCO, 2019). There is mounting evidence that only a small subset of cancer cells within a heterogenous tumor have metastatic capability — known as breast cancer stem cells (BCSCs). Literature suggests that BCSCs contain an overactivation of the Wnt signaling pathway and that it is integral to their metastatic and tumor growth capabilities. Wnt overactivation in BCSCs, defined by their CD44+ phenotype, manifests as the up-regulation of the LRP6 co-receptor on the cell surface (Liu, 2010). LRP6 provides an important potential therapeutic target for BCSC treatment and LRP6 silencing in breast cancer has been previously shown to reduce cell proliferation and tumor growth. Previously, Dr. Goswami's lab has shown the effectiveness of a monoclonal antibody 2F1 (2F1) —specific for the E1E2 domain of LRP6 — through in-vitro studies. In this study, 2F1 was examined for its ability to inhibit Met-1 mammary cancer progression in-vivo. The Met-1 cell line is known to progress in the stepwise manner characteristic of human breast cancer.

Utilizing the MMTV-PyMT mouse model, 2F1 was evaluated for its ability to inhibit Met-1 tumor growth and metastasis in comparison to a chemotherapy standard Doxorubicin (Dox) and a small molecule LRP6 inhibitor Salinomycin. Palpable Met-1 tumors were generated in FVB mice through intraperitoneal injection. Over a 5-week treatment period, mouse trial groups (n=5) were treated with once-a-week injections of Doxorubicin (2mg/kg), Salinomycin (5mg/kg), or 2F1 (5mg/kg). Tumor growth inhibition was analyzed through observation of FVB mouse tumor size and graphical/pairwise analysis. Metastasis prevention was determined through qRT-PCR analysis of PyMT oncogenic expression in lung and bone marrow tissue. The results of these experiments show that 2F1 significantly reduces both tumor growth and Met-1 metastasis, and thus is capable of LRP6 silencing at a 5mg/kg concentration in-vivo. This suggests that 2F1 and, more generally LRP6 silencing with monoclonal antibody therapy at the cell surface, can be potential therapeutic targets in breast cancer treatment.

This research introduces the monoclonal antibody 2F1 as a promising antitumor and antimetastatic treatment and lays the foundation for its utilization as a breast cancer targeted therapy for patients with tumor overexpression of LRP6. Future studies will focus on human breast cancer cell lines in an immune compromised SCID mouse models to further concretize the effectiveness of 2F1 and better signify its potential performance in clinical trials. Additionally, an extension study involving surgical removal of the tumor before therapy administration may provide more translational results.

Background and Introduction

Aside from skin cancers, breast cancer is the most commonly diagnosed cancer in American woman with 300,000 Americans diagnosed each year (ASCO, 2019). Over the past three decades, the mortality rate of primary non-metastatic breast cancer has consistently declined due to early detection, improved screening, increased awareness, and novel therapeutic options. However, once breast cancer advances to metastatic breast cancer there are few effective treatment options. Metastatic breast cancer comprises the vast majority of breast cancer related deaths and individuals with metastatic breast cancer have a 5-year survival rate of 27% (ASCO, 2019). Representative of all cancers, metastasis is a multistep process that begins with invasive behavior at the primary tumor site and systematic intravasation of tumor cells into the blood stream, leading to extravasation out of the vessel and tumor cell invasion at a distant secondary location while retaining proliferating capabilities. Specifically, in regard to breast cancer, an aggressive variant of the disease occurs in ~10% to 15% of patients and metastasizes within three years of diagnosis (Robinson, 2009). Still, traditional non-aggressive breast cancer patients remain subject to a high-risk of developing breast metastatic disease throughout the course of their life — manifestation of metastatic disease can emerge from traditional primary tumor origins ≥10 years after initial diagnosis (Robinson, 2009). Appropriately, breast cancer research has shifted to focus more specifically on the metastatic breast cancer with the goal of understanding metastatic markers and discovering potential treatment pathways.

There is mounting evidence that metastatically capable cells are distinct from typical tumor cells. Only a small subset of cancer cells within a heterogenous tumor have metastatic capability — known as breast cancer stem cells (BCSCs). BCSCs have been proven to be highly invasive, non-proliferating cells that exhibit apoptotic and cytotoxic therapy resistance. BCSCs exhibit stemness that sustain cancer progression and have enhanced capacities for self-renewal, cloning, metastasizing, homing, and reproliferating (Liu, 2010). Similar to adult somatic stem cells, BCSCs divide asymmetrically to create both one daughter progenitor cell— that drives tumorigenesis — and one self-renewing BCSC (Aponte, 2017). They are thought to originate from a combination of somatic oncogenic mutations and environmental factors that cause *de novo* de-differentiation, leading to development of stem properties (Sin, 2017). The origin of BCSCs is still not well understood and remains a topic for further research.

Within the physical breast tumor, BCSC are vastly outnumbered by nontumorigenic cancer cells. BCSCs and nontumorigenic cancer cells share much of their genetic and phenotypical expression, making it difficult to differentiate between the two. Thus, there is a need for nuanced BCSC markers. Multiple cancer stem cells markers have been identified in the past two decades, the most significant of which is cell surface markers CD44 and CD24. The CD44+/CD24- phenotype of cells has shown increased tumorigenicity, stem-like properties, and has been used extensively to isolate BCSCs (Al-Hajj, 2003). As few as 10 cells that exhibited the CD44+/CD24- phenotype have been shown to successfully propagate metastasis while upwards

of 10,000 cells lacking the phenotype were unable to lead to successful metastasis (Liu, 2010). Cells that are CD44+/CD24- are metastatically capable, aggressive, and support the belief that BCSCs are central to breast cancer metastasis.

Importantly, CD44+ expression indicates the overactivation of the Wnt signal transduction pathway. CD44 is a major Wnt pathway target gene and a strong correlation between CD44 and Wnt expression has been found (Reya, 2005). Specifically, CD44 acts as a positive regulator of the Wnt receptor complex — CD44 overexpression increases Wnt activity in a concentration-dependent manner (Schmitt, 2015). Wnt overactivation is inherent to CD44+ breast cancer and the canonical Wnt signaling pathway has emerged as a critical regulator of cancer stem cells (Reya, 2005).

The Wnt signaling pathway is an evolutionary conserved signal transduction pathway involved in cell cycle regulation and stimulation. In addition to its relationship with carcinogenesis, it has been shown to play a substantial role in embryogenesis, regulating crucial aspects of cell fate determination, cell migration, cell polarity, neural patterning and organogenesis during development (Yuko, 2008). There are two main Wnt pathways — the canonical pathway (Wnt/β-catenin dependent) and the non-canonical pathways (Wnt/β-catenin independent). The canonical Wnt pathway, which controls regulation of gene expression and cell proliferation, is directly implicated in carcinogenesis and is activated by Wnt-protein ligands. Wnt ligands are comprised of 19 secreted glycoproteins that are found in the immediate extra-cellular environment through paracrine or juxtracrine excretion. Mechanistically, ligand binding occurs at the low-density lipoprotein receptor-related protein 6 (LRP6) and activates the Frizzled/LRP5/6 complex. Activation of this protein complex triggers a series of events that disrupts the APC/Axin/GSK3 complex, blocking downstream phosphorylation and inhibiting proteasomal degradation of β-catenin (Komiya, 2008). The overproduction of β-catenin then activates downstream target genes which induce cell proliferation, survival characteristics, and self-renewal capabilities. Stemness resulting from Wnt activation is still being explored, but recent research points to the increased telomerase activity detected upon β-catenin triggering as a potential explanation (Hoffmeyer, 2012).

Although the complete mechanism regulating BCSC self-renewal is not well understood, there is strong reason to support the hypothesis that self-renewal is mediated by the Wnt signaling pathway and that elevation of its expression in BCSCs directly allows for tumorigenesis and metastatic proliferation. Wnt overactivation in BCSCs, defined by their CD44+ phenotype, manifests as the up-regulation of the LRP6 co-receptor on the cell surface (Liu, 2010). With increased copy numbers compared to healthy somatic cells and non-tumorigenic cancer cells, LRP6 provides an important potential therapeutic target for BCSC treatment. LRP6 silencing in breast cancer has been shown to reduce Wnt signaling and thus cell proliferation and in vivo tumor growth. Local administration of Mesd, a LRP6 antagonist recombinant protein, has

successfully inhibited both breast cancer tumorigenesis in-vivo and significantly decreased metastatic invasion in triple negative breast cancer lines (Ma, 2017). Ma's research with Mesd reinforces LRP6's role in both tumorigenesis, metastasis, and provides a foundation for future LRP6 BCSC targeted therapies.

The small-molecule selective inhibitor Salinomycin is the first drug reported as a selective cancer stem cell inhibitor. Salinomycin functions to block the phosphorylation of LRP6 and signals for its degradation. Application of Salinomycin as a LRP6 targeted therapy has shown to reduce cancer stemness expression in leukemia (Lu, 2011)(Gupta PB, 2009). Recently, Gupta et al. discovered that Salinomycin selectively kills BCSCs. However, as a small-molecule therapy Salinomycin lacks specificity and is prone to induce harmful non-target effects.

Monoclonal antibody (Mab) therapies are biological therapies that provide highly specific targeting and reduced side-effects. Because of their high efficacy and untapped potential, biologics-based drugs such as Mabs are at the forefront of biotechnological advancement and drug development. Although Mab targeted therapy of LRP6 has been previously unexplored in breast cancer, it has been used to halt the Wnt pathway for treatment of diabetic retinopathy. Mab 2F1 (2F1) is a monoclonal antibody developed to be specific to the E1E2 extracellular domain of the LRP6 receptor (Zhou, 2010). Analysis of 2F1 in the context of diabetic retinopathy has shown robust inhibition of the canonical Wnt signaling pathway both in vitro and in vivo studies (Lee, 2012). Translation of 2F1 toward a cancer therapy is promising and evaluating 2F1 in the context of BCSCs is the primary focus of this study.

The current standard for breast cancer treatment is surgical removal of the tumor and then administration of neoadjuvant and adjuvant chemotherapy. A prevalent chemotherapy used is Doxorubicin (Dox) — an anthracycline and chemotherapeutic drug with high anticancer activity (Zhao, 2017). The goal of Dox treatment is to prevent tumor recurrence and metastasis, and it is associated with a clinical benefit of 3% to 10% increase in 15-year survival (Robinson, 2009). Used as a blanket therapy administered in the majority of cancers, Dox has been shown to be effective in tumor reduction. However, BCSC's acquired chemoresistance renders Dox treatment less effective for metastatic cases. Adverse reactions are common with Dox treatment and acute cardiac toxicity is a significant additional side effect to the fatigue, alopecia, nausea and vomiting, and oral sores standard in most chemotherapies (Johnson-Arbor, 2020). The lack of specificity and plethora of side-effects inherent to Dox treatment has created a noticeable clinical need for improved targeted therapies able to treat BCSCs. In this study, Dox was administered in tandem with other therapies to mimic how it is administered in the clinic.

Metastatic cancer research is dependent on implementation of effective model systems. Much of the existing knowledge of metastasis has been derived from the use of in-vivo experimental mouse models. Although a mouse model that accurately replicates metastasis from initial

carcinogenesis to end-stage metastatic disease is yet to be identified, the MMTV-PyMT model has proven to effectively simulate human metastatic breast cancer (Borowsky, 2005). The effectiveness of this transgenic mouse model comes from the use of the mouse mammary tumor virus (MMTV) promoter to express the polyoma middle T antigen (PyMT) on mammary epithelial cells, producing a malignant transformation analogous to the human disease (Werbeck, 2014). Cells derived from mammary carcinomas of MMTV-PyMT FVB mice, named Met-1 cells, are known to progress in the stepwise manner characteristic of human breast cancer and have been characterized as highly metastatic. Met-1 cells have been shown to exhibit invasive growth and metastasis in the lung ~99% of the time they are injected into the mammary fat-pad of female FVB- mice and lead to lung metastases by 20 weeks of age (Werbeck, 2014)(Borowsky, 2005). Therefore, the Met-1 cell line and the MMTV- PyMT breast cancer FVB mouse model provides reliable and reproducible procedure for investigating metastasis and molecular components of breast cancer in-vivo.

Materials and Methods

FVB Mice and Injection of Met-1 cells

All animal studies were done under a protocol (YC-BIO 2008/2007) approved by the National Cancer Institute, in accordance with Association for Assessment and Accreditation of Laboratory Animal Care Guidelines. The 20 female FVB mice used in this study were acquired from the YC Biology department breeding initiative. Thanks to the help of Raymond Reynoso of the biology department, FVB mice were breed and their pups were separated by sex 3 weeks after birth. When they reached 6 weeks of age, female FVB mice were processed and grouped for the experiment.

The 20 female FVB 6-week-old mice were inoculated with Met-1 cells (mammary cancer cell line bearing the PYMT gene) in order to develop highly metastatic mammary tumors — expected to form a palpable tumor after 7 days (Liu, 2010). This was accomplished by injection $1x10^6$ Met-1 cells intraperitoneally into the left uppermost mammary fat pad of each mouse. Met-1 injection followed the subsequent approved protocol: an individual FVB mouse was selected and placed in the isoflurane device under a fume hood. The mouse was then anesthetized as per YC protocol — using 3% isoflurane gas induction and maintained at 2% isoflurane exposure for an interval of 2-5 minutes. The mammary fat pad of the anesthetized mouse was then sterilized by application 70% ethyl alcohol around the nipple area. A 25-guage (G) needle was then filled with a prepared solution of $1x10^6$ Met-1 cells in 100ul of PBS. First, MET-1 cells were cultured in YC cell culture facility. Cell culture was done by Dr. Gargi Bandyopadhyaya. Approximately $7x10^6$ Met-1 cells were cultured and total cells were diluted so that each mouse will get $1x10^6$ Met-1. Injection commenced by inserting the needle shallowly underneath the target nipple so that only 2mm of the needle was internal and slowly pressing to release the 100ul of solution. After inoculation the mouse was then returned to its cage and randomly assigned to one of four groups (n=5); control, Doxorubicin (Dox), Dox + Salinomycin (Dox+Sali), and Dox + 2F1 (Dox+2F1).

For the length of this 45-week investigation, mice were handled following the YC-BIO protocol as described below. Mice were held in a Tecniplast Deluxe Reusable Animal cage, fed BioServ Rodent Diet, and kept on Ancare NESTLETS NESTING MATERIAL-MICE bedding (as specified in YC-BIO 2008/2007). The mice were housed in the YC animal facility that had a facility temperature was kept between 21 °C and 22 °C. Each cage contained 2-3 mice that were checked every second day to ensure the health of the animals. At the end of the week the mice were transferred to new clean cages with replenished food and water. The used cages were then adequately cleaned and sterilized to be reused in consequent weeks. When a mouse was found deceased, it was properly disposed of in a toxic waste bag and placed in the appropriate place in the biology floor as designated by the YC-BIO protocols.

Treatment of MET-1 Tumors

Palpable tumor formation was expected to occur within 7-10 days of the original inoculation date (Guy, 1992). To standardize the data, a palpable tumor was defined as 4mm in diameter.

Palpable tumors were expected to appear ~ 4 weeks after inoculation (Guy, 1992). Once a palpable tumor was present and measured to be of sufficient diameter, the appropriate treatment was administered (as defined by their respective groups, protocol defined below). Each treatment was administered through an injection intraperitoneally. When a treatment group required two different drug injections — as was the case with the Dox + Salinomycin and Dox + 2F1 groups — they were given on separate, consecutive days to avoid discomfort in the animals and ensure drug effectiveness. After five weeks of treatment, the mice were euthanized using carbon dioxide as per YC animal protocols (described below). A mouse that perished prior to the completion of the 5-week treatment timetable was disposed of properly and noted appropriately.

Doxorubicin treatment was administered to the Dox (n=5), Dox + Salinomycin (n=5), and Dox + 2F1 groups. The Doxorubicin was purchased from Cayman Chemicals as 25mg solid stock and was prepared under sterile conditions. The solid was then diluted 1:1000 in PBS to create a stock solution and handled as per manufacturer's instructions. The dosage of 2mg/kg was chosen as an effective chemotherapy level that ensured survivability (Aston, 2017). The mice were anesthetized as per previously mentioned YC protocol and Dox injections were given using a 20G syringe inserted intraperitoneally under a pinched area of the skin of the abdominal region. Pinching technique of the skin was suggested by Dr. Goswami and consisted of pinching and stretching the skin using either forceps or the index and thumb finger, allowing for seamless intraperitoneally injection.

The anti-LRP6 monoclonal antibody 2F1 treatment was administered to the Dox + 2F1 group (n=5) on the following day as the Dox treatment was given. The targeted antibody was acquired generously from Dr. Ma's Lab, *Department of Physiology and Harold Hamm Diabetes Center, University of Oklahoma, Health Sciences Center, Oklahoma City, Oklahoma*, in which they generated the antibody through use of a recombinant peptide comprising the E1E2 domain of LRP6. The antibody acquired was purified through affinity chromatography protein G and dialyzed against PBS by Dr. Gargi Bandyopadhyaya, a secondary investigator in Dr. Goswami's laboratory. A dose of 5mg/kg of 2F1 was decided to be effective in-vivo based on the dosage used in diabetic retinopathy research (Lee, 2012). The 2F1 was made to a dilution whereby 5mg/kg was given in 100ul injection. The mice were anesthetized as per previously mentioned YC protocol and 2F1 injections were given using a 25G syringe inserted intraperitoneally under a pinched area of the skin of the abdominal region. A 25G syringe was used to ensure the integrity of the antibody and reduce pressure levels as the solution moves out of the needle.

The anti-LRP6 small molecule Salinomycin treatment was administered to the Dox + Salinomycin group (n=5) on the following day as the Dox treatment was given. The molecule was bought from Sigma-Aldrich at a quantity of 2mg. A dose of 5mg/kg of body weight was shown to be effective in-vivo in leukemia research by Dr. Lu and implemented to this study (Lu, 2011). The dosage was prepared by Dr. Gargi Bandyopadhyaya and made to a dilution whereby a 20g mouse received 100ul injection. The mice were anesthetized as per previously mentioned YC protocol and Salinomycin injections were given using a 20G syringe inserted intraperitoneally under a pinched area of the skin of the abdominal region.
Control group did not get any chemotherapeutic treatment. Tumor measurement were performed as per other three groups.

At the completion of the 5-week study, the surviving mice were euthanized as per the YC-BIO 2008/2007 protocol standards. Carbon dioxide was implemented as the humane method of euthanasia and mice were deposited in a carbon dioxide chamber and euthanized with 100% CO_2. The corpses were then analyzed within the lung and bone marrow metastasis protocol. After completion, they were then disposed of as per YC-BIO 2008/2007 standards. When a mouse died prior to the completion of the study, they were analyzed and disposed of in the same way.

Tumor Size Data Retrieval

Beginning one week after the first injection, the tumor size was measured weekly using standard external calipers. Measurements were taken by holding the mouse by the nape of its neck and placing the end of the caliper on both sides of the tumor. The smallest longitudinal length of the palpable mass was recorded in Table 1. To combat the possibility of necrotic volume distorting the tumor size readings, measurements were only taken of the hard parts of the tumor and the soft sections were ignored. Only obvious spongey masses were deemed necrosis rather than tumor. Mice that perished prior to the end of their treatment plan had their tumors measured prior to their metastasis analysis and disposal.

Lung and Bone Marrow Metastasis Extraction

Extraction of the lung and bone marrow for metastasis analysis was done on the same day of the mouse's death. Lung extraction protocol below was taken from John Morton's protocol and incorporated to follow the YC-BIO 2008/2007 standards.

Lungs were stored in 10% formalin (a known lab fixative for preserving animal tissue). After euthanasia, the mouse carcass was secured to a dissecting board using pins. The mouse was positioned dorsally with full extension of pelvic and pectoral limbs and soaked with 70% ethanol using a spray bottle to keep hair out of the way while dissecting. The skin over the sternum was then grasped with forceps and an initial incision was made at the ventral midline. The incision was continued cranially and caudally along the ventral midline to extend from the chin to the pubis. The skin was gently reflected bilaterally at the ventral midline incision extending from the ventral thorax to the abdomen, completely exposing the thorax and abdomen. A ventral midline incision was then made into the abdomen to expose the peritoneal cavity and the sternum. Scissors were used to cut the ribs on each side of the sternum at about the mid-level of the body of the ribs. The diaphragm muscle was then cut with a scalpel in an amount sufficient to release it from the rib portions to be removed. Subsequently, the rib cage was then removed to expose the entire thoracic cavity. Care was taken not to damage the lungs while cutting. Pulmonary tissue of each lobe was then removed using forceps and pulling the lobes free from the trachea. The lobes were then placed in the vial prepared earlier. The lobes were then transferred to the -80º freezer to be stored until qRT-PCR analysis occurred (Morton, 2017). The mouse was then left to undergo bone marrow extraction.

Bone marrow metastasis extraction followed the below protocol that relied on YC-BIO 2008/2007 standards.

The femur was removed from the pinned carcass using scissors and making an incision at where the femoral head and pelvis met. Residual tissue, hair, and skin were then cleaned off using forceps and ethyl alcohol. Two more incisions were then made at the neck of the femur and the patella of the knee, creating two porous openings in the bone. 200 ul of PBS buffer was then filled into a pipette and injected into the neck of the femur at the incision point 100ul at a time. The tip of the pipette was held steadily on the opening to ensure that the solution ran through the bone and expunging its contents at the patella, rather than escaping to its sides. The 200ul of flow-through was collected in a vial. 1500ul of 1x RBC Lysis Buffer (five times the volume of sample) was added to the vial and placed in an ice bath for 20 minutes. The sample was then centrifuged at 1000 rpms for 10 minutes at 4° C (cold centrifuge). The resulting supernatant was removed using a pipette and the remaining pellet was labeled and stored in -80° freezer.

Preparation of Lung and Bone Marrow for qRT-PCR Analysis

The collected lung tissue and bone marrow cells were collected from the liquid nitrogen and prepared for qRT-PCR analysis through DNA extraction and PCR amplification techniques. DNA extraction of lung tissue and bone marrow was accomplished through the following protocol adopted from Applied Biosciences DNA/RNA Extraction Kit. Materials were also acquired from the kit.

The frozen lung was removed and placed in a standard sized mortar and pestle. Liquid nitrogen was added to cover the tissue. 15 seconds was waited for the tissue to solidify. The tissue was then ground with the pestle until it was a fine powder. 300uL of PBS was then added to the mortar and it was made sure that all the powder was dissolved in the solution. The 300uL solution was then transferred to an Eppendorf tube using a 1000p pipette. Equal volume of DNA/RNA lysis buffer (300uL) was added to the Eppendorf tube, bringing the solution to 600ul. The solution was then transferred into a yellow Spin-Away Filter from the DNA/RNA Kit and ready for DNA extraction.

The bone marrow pellet was retrieved from the freezer and 200uL of DNA/RNA lysis buffer was added and mixed well. The solution was then transferred into a yellow Spin-Away Filter from the DNA/RNA Kit and ready for DNA extraction.

The yellow Spin-Away Filter from the DNA/RNA Kit containing either lung sample or bone marrow sample was centrifuged at 1000 rpm for 1 minute. The column of the Yellow Spin-Away Filter was then transferred to a new collecting tube and 400uL DNA/RNA Prep Buffer was added to the column. This new column was then centrifuged at 1000 rpm for 1 minute. Both the collection tube and the flow-through it contained was discarded and a new collection tube was attached to the column. 700uL DNA/RNA Wash Buffer was then added and centrifuged for 1 minute at 1000 rpms. Both the collection tube and the flow-through it contained was discarded and a new collection tube was attached to the column. 400uL DNA/RNA Wash Buffer was added to the new column and centrifuged for 2 minutes at 1000 rpms. Both the collection tube and the flow-through it contained was discarded and a new collection tube was attached to the column. 100uL DNase/RNase-Free-Water was added directly to the column matrix. After waiting for 5 minutes, this sample was centrifuged for 1 minutes at 10000 rpm to elute the DNA from the matrix into the collecting tube.

To ensure adequate DNA quantities in the sample, the collected sample was analyzed using a Nanodrop 1000 (ThermoScientific, 2012). The machine was blanked using dH_2O before use. 2uL of the DNA sample was placed on the machine pedestal. The sample was then analyzed using the ND-1000 software for measuring RNA/ DNA yield (ng/ul) and RNA/DNA purity (A260/280). A 260nm to 280nm value is a ratio of absorbance values that determines sample purity. For this investigation, a 260/280 range of 1.8-2.3 was determined to be acceptable purity (Thermo Scientific, 2012).

PyMT Gene Amplification of the Extracted DNA Accomplished Using PCR

The extracted DNA was amplified through the use of PCR to increase the PyMT copy number. PyMT is the indicator gene for metastatic occurrence. The PCR 200 ul solution was prepared in order to incorporate a larger amount of initial sample DNA. The PCR was prepared with the following specifications: 100uL Immomix, 10uL $MgCl_2$ (calculated to be 5%), 10uL of 10uM PyMT Primer, 600ng DNA volume calculated specific to each Nanodrop value, and Nucleus Free Water to reach 200ul. The sample was then run in EdvoCycler™ set to cycle 45 and melting temperature 60 degrees centigrade. 600ng of DNA was determined to be the amount of DNA necessary to acquire a sensitivity of 1 metastatic cell in 100,000 healthy cells (Fellowes, 2012). This was extrapolated from the fact that 1 cell has 6 picogram of DNA and thus to include enough DNA for this sensitivity 600,000 picograms (600ng) is needed. Therefore, with 600ng of lone or bone marrow DNA added to the PCR, PyMT will be detected at a standard of 1 to 100,000 cells present.

The 200ul PCR sample was then purified using a Qiagen brand PCR purification kit. This removed the residual primers from the PCR cycle, leaving only the PyMT amplified DNA to be used in the qRT-PCR.

Metastasis Detection of Lung Tissue Through qRT-PCR

After purification, the 200ul PCR sample was diluted 1:10,000x to generate the 10ng/ul concentration necessary for qRT-PCR. Quantitive real-time PCR, (qRT-PCR) is a laboratory technique that monitors the amplification of targeted DNA molecule during PCR through recognition of a fluorescent probe. qRT-PCR enables quantification of gene expression in the samples being tested. The below qRT-PCR protocol was adopted from ThermoFisher Scientific SYBR Green Real-Time PCR Protocol (ThermoScientific, 2019).

 qRT-PCR was accomplished using master mixes A and B. Master mixes were designed for each lung to have 3 replicates and created with the following specifications (quantification of master mixes were done with a 4-replicate group in mind to create excess in case an issue arose). Master Mix A (MMA) contained 4ul of Lung DNA with 20ul Sybergreen (expounded from the standard 1uL DNA with 5uL Sybergreen standard protocol). Master Mix B (MMB) contained 4uL of 2.5 uM PyMT Primer with 12uL Nucleus Free Water (expounded from the standard 1uL DNA with 5uL Sybergreen standard protocol). After the mixes were prepared, they were inserted into a 8-well qRT-PCR microtube plate in the following manner. 6ul of MMA was pipetted into wells 1-3 followed by 4ul of MMB into wells 1-3 resulting in a volume of 10uL.10ul of chilled wax was then added to each tube using proper sterile pipetting technique. The microtubes were then

centrifuged and placed in the qRT-PCR machine for analysis. Sybergreen was kept in the dark throughout the entire procedure.

Lung and Bone Marrow qRT-PCR Analysis

 qRT-PCR reagents with DNA from both lung and bone marrow were run in the Applied Biosystems 7300 Real-Time PCR System. The qRT-PCR reaction condition was set according to the below Applied Biosciences specifications (Diagram 1 below). First, the wells were exposed to 50.00º for 2 minutes for activation of the housed DNA. Next, they were subjected to a 40 cycle PCR reaction sequence entailing: denaturation of double stranded DNA at 95°C for 15 seconds, primer annealing of DNA at 58°C for 30 seconds, and extension of the DNA strand at 72°C for 30 seconds. Fluorescent reading of Sybergreen was read at the 72°C extension step. This was followed by melt curve generation sequence. Moreover, the reactions were normalized against the GAPDH housekeeping gene to generate ΔΔCt values. Data was reported as the ΔΔCt at a standardized fluorescence intensity level for PyMT gene expression compared first to GAPDH and then to the control cell line.

<u>1</u>	<u>2</u>	<u>3</u>	<u>4</u>	<u>5</u>
50.00º for 2 minutes	95.00 for 10 minutes	95.00 for 15 seconds 58.00 for 30 seconds	72 for 30 seconds	Dissociation Melt Curve Generation
Repeated 1x	Repeated 1x	Repeated 40x	Repeated 1x	Repeated 1x

Diagram 1: qRT-PCR Setup *Reaction conditions for qRT-PCR steps 1-5.*

Mouse Survivability and Timeline

Met-1 injections were successful in creating palpable tumors in all 20 female FVB 6-week-old pups. No noticeable complications were found from intraperitoneal injections. After four weeks of inoculation, all mice were started on their designated treatment regimen with tumor size data recorded in table 1 below. At the end of the 45-week trial, 19 mice were still living and needed to be euthanized. A single mouse died prior to the completion of their treatment — succumbing to the cancer between week 4 and 5 injections. Death of specimen in this model is common and was treated as an indicator of error.

Animal Group	Week 0 Tumor Size (mm +/- 0.5mm)	Week 1 Tumor Size (mm +/- 0.5mm)	Week 2 Tumor Size (mm +/- 0.5mm)	Week 3 Tumor Size (mm +/- 0.5mm)	Week 4 Tumor Size (mm +/- 0.5mm)	Week 5 Tumor Size (mm +/- 0.5mm)
Control	4	5	8	15‡	30‡	21‡
	3.5	8	9	15	17	23
	4	8	14	11	17	24‡
	4	6	12	12	16	24‡
	3.5	8	12	18‡	22‡	23‡
Dox	4	7	9	11	12	8‡
	3.5	8	9	11	10‡	15‡
	4	7	8	10	8	8
	4	8	9	9	10	10‡
	3.5	6	8	17‡	12‡	10‡
Dox+Sali	4	8	15	10	11	11‡
	4	8	9	11	10	11
	3.5	5	8	11	11‡	7‡
	4	12	7	10	9	8
	4	5	7	8	9.5	n/a
Dox+2F1	3.5	12	5	9	7	4
	4	9	6	12	8	3
	3.5	5	6	7	7	3
	4	5	7	9	8	8‡
	4.5	5	6	8	8	8

Table 1: Tumor Size Raw Data Smallest longitudinal diameter was recorded for each mouse using a standard caliper and technique described in materials section. ‡ indicates the presence of noticeable necrotic inflammation within the palpable tumor. The necrotic portions were ignored in such cases and only the firm parts of the tumor measured. n/a indicates a mouse that died prior to completion of injection treatment.

At the onset of treatment, the groups were observably similar in behavior and appearance. However, by week 3 there were noticeable differences beginning to occur to both the behavior of

the mice and the tumors being measured. In the Control group, mice were less active and more docile than the other groups. By week 4, the control group was noticeably consuming less feed (as seen by the amount remaining during weekly cage changing). Necrosis was also first observed in week 3 for both Control and Dox groups. Necrosis became more prevalent as tumors developed and the majority of Control, Dox, and Dox+Sali mice had necrotic masses by the completion of the study. The Dox+2F1 group had only one mouse develop necrosis, which occurred down the line in the final week of treatment. At the completion of 5 weeks of treatment, all mice were consuming smaller amounts of feed and behaved lethargically. Only one mouse, in the Dox+Sali group, did not complete the treatment plan. The metastasis evaluation was done to that mouse the day it died — the data was included with the rest of the metastasis data.

Mab 2F1 Treatment Reduces MET-1 Tumor Size Significantly
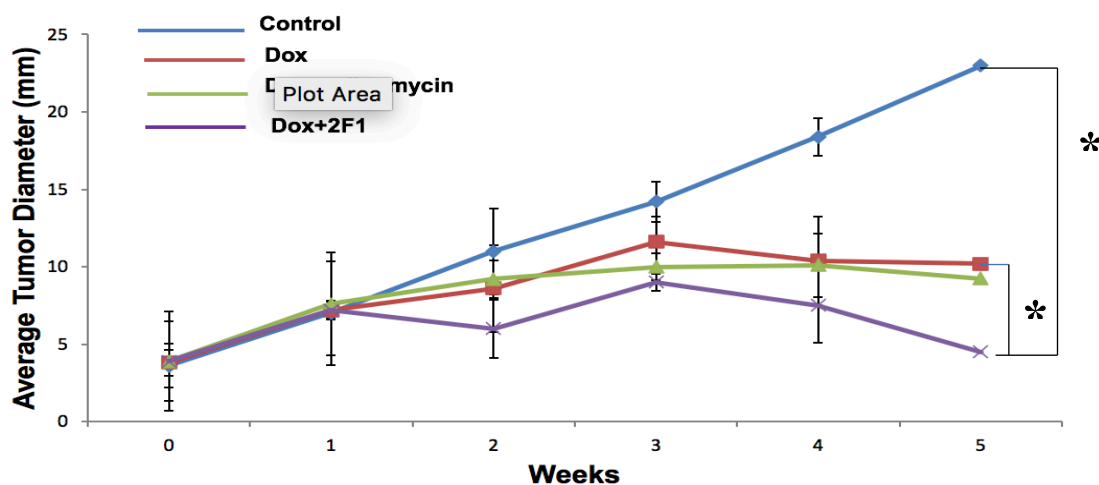
Animal	Week 1 Average Tumor Size (mm)	Week 1 SD	Week 2 Average Tumor Size (mm)	Week 2 SD	Week 3 Average Tumor Size (mm)	Week 3 SD	Week 4 Average Tumor Size (mm)	Week 4 SD	Week 5 Average Tumor Size (mm)	Week 5 SD
Control	7	1.41	11	3.33	14.2	2.77	18.4	1.32	23	1.22
Dox	7.2	0.83	8.6	0.54	11.6	2.8	10.4	1.63	10.2	2.86
Dox+Sali	7.6	2.57	9.2	3.34	10	1.22	10.1	0.89	9.25	2.06
Dox+2F1	7.2	3.19	6	0.63	9	1.87	7.5	0.57	4.5	2.38

Figure 1: Met-1 Tumor Growth Over 5-Week Treatment Period *Met-1 Tumors in FvB mice were injected with Dox (2mg/Kg), Salinomycin (5mg/kg) and 2F1 (5mg/kg) for 5 weeks. Averages and standard deviations for each week were calculated and graphed to show Met-1 progression. The data points are found in the above table. Selective pairwise comparisons run for each treatment group showed statistical significance of Dox+2F1 group compared to Control, Dox, and Dox +Sali groups, indicated by *. N=5, *= p < 0.05.*

Raw data from table 1 was analyzed to determine the inhibition ability of each treatment and conclude significance between treatment options (Figure1). The data for each week was averaged and standard deviations were found. Figure 1 shows the graphical analysis of the data. Control has a significantly more consistent growth trend that is considerably greater than that of the other treatment groups. Prior to week 3, all four treatment groups have similar data trends

with overlapping standard deviations. As treatment moved past week 3, tumor size began to behave differently for each group. Control group tumors continued to grow at a similar pace as the first 3 weeks, but the Dox and Dox+Sali groups began to flatten out and maintain a similar tumor size to week 3 for the rest of the study (Dox: 11.6mm in week 3, 10.2 in week 5; Dox+Sali: 10mm in week 3, 9.25mm in week 5). The Dox+2F1 treatment group began to noticeably reduce tumor size starting week 3 and by week 5 had an average tumor size of 4.5mm — 4.75 mm smaller than the next smallest week 5 average and 18.5mm less than Control. Dox and Dox+Sali data shows the two groups reacting similarly to their treatments. The two groups were at least within 1.6mm of average tumor size in each week and have visually similar trend lines in Figure 1. Standard deviations for the week averages were consistent throughout each group and no outliers were determined to be present. The speed of treatment activation and impact of dosage used are aspects that need to be further investigated.

To determine significant difference in the data, the open-access web tool *TumGrowth* was used. Standard statistical analysis, such as a Students T-test, cannot be applied to tumor growth curves due to their longitudinal nature and small sample size. Created by Kroemer Lab for experimenters with limited statistical knowledge, *TumGrowth* provides an R package software tool that enables a series of statistical comparisons across or between groups of tumor growth curves obtained in a standard laboratory (Enot, 2018). Pairwise comparisons of the four treatment groups were run using the help of the *TumGrowth* software, as seen in Figure 2. Pairwise comparison is the most accurate way to determine p-value for tumor growth.
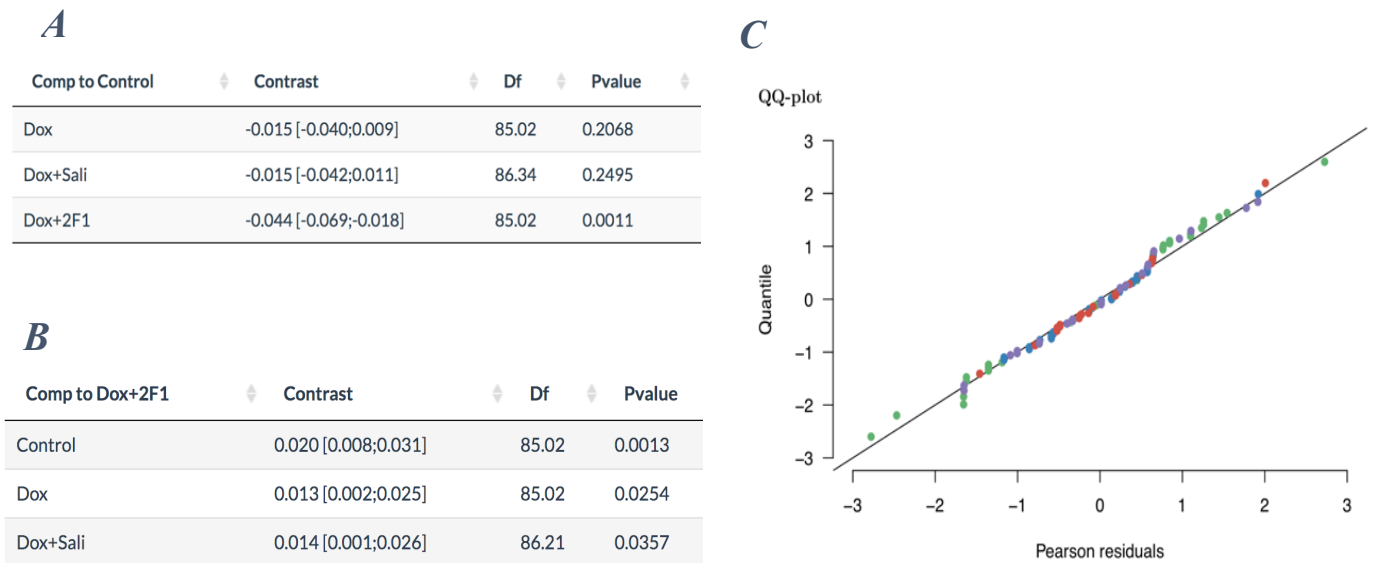
A

Comp to Control	Contrast	Df	Pvalue
Dox	-0.015 [-0.040;0.009]	85.02	0.2068
Dox+Sali	-0.015 [-0.042;0.011]	86.34	0.2495
Dox+2F1	-0.044 [-0.069;-0.018]	85.02	0.0011

B

Comp to Dox+2F1	Contrast	Df	Pvalue
Control	0.020 [0.008;0.031]	85.02	0.0013
Dox	0.013 [0.002;0.025]	85.02	0.0254
Dox+Sali	0.014 [0.001;0.026]	86.21	0.0357

C

Figure 2: Pairwise Comparison of Raw Data *Pairwise statistical analysis was run using the TumGrowth software to determine statistical significance. p < 0.05 was considered to be significant. **(A)** Pairwise comparison of Dox, Dox+Sali, and Dox+2F1 data to control values with p-values recorded in rightmost column. **(B)** Pairwise comparison of Dox, Dox+Sali, and control data to Dox+2F1 values with p-values recorded in rightmost column. **(C)** QQ Plot shows how effective the statistical analysis transformation done correlates with original data. Data points should lie as close to the straight line as possible. The graph here shows no significant deviations from the line and corroborates the methods used.*

TumGrowth analysis shows consistent and significant reduction of tumor growth of Dox+2F1 group when compared to the control (p = 0.0011, Figure 2A). Interestingly, there was no significant difference of tumor growth reduction of Dox and Dox+ Sali treated groups when compared to the control group (p > 0.05). Notably, a significant difference was found when Control (p = 0.0013), Dox (p = 0.0254), and Dox+Sali (p = 0.0357) groups were compared to Dox+2F1 (Figure 2B). Therefore, the data supports the conclusion that 2F1 antibody played significant role in tumor growth reduction compared to previous standards. Additionally, the negligible difference between Dox and Dox+Sali data shows Salinomycin was ineffective at the dosage in the FVB mice model. This could indicate that Salinomycin had no additional impact to singular Dox treatment.

Dox+ 2F1 Inhibits Lung and Bone Marrow Metastasis

For metastasis analysis, first DNA was extracted from lung and bone marrow. This was done on the same day of the mouse's death for all 20 FVB mouse in the study. Visible metastasis masses were consistently visible in control lung tissue and did not visually appear in the Dox, Dox+Sali, and Dox+2F1 lung tissue. No visible metastasis was seen on any mouses fibula during bone marrow extraction.

DNA extraction and PCR amplification of PyMT gene was run and samples were recorded and adjusted accordingly to ensure the 600ng sample minimum. Sample purity was also determined through use of Nanodrop and all samples generated a 260/280 value between 1.7-2.3, constituting them adequately pure for analysis.

Preparation of mouse DNA for qRT-PCR was successful for both bone marrow and lung tissue samples. ΔCt values for both Lung and bone marrow tissue were analyzed to determine the relative amount of PyMT genetic expression. ΔCt values found correlate to relative PyMT genetic expression in the collected cells, indicating if metastasis had reached the observed tissues. As stated earlier, data from qRT-PCR reported as ΔCt normalized to the housekeeping gene GAPDH. Furthermore, ΔCt gene expression for the control group was set as 1 in reference to the Dox, Dox+Sali, and Dox+2F1 values. This allowed the data to be displayed as a relative amount of expression compared to the control, as seen in in figure 3. Relative amount compares the variation of the expression of the PyMT target gene between treatment groups. A Students T-test was run to determine significant difference between the treatment groups, with p< 0.05 as the confidence threshold.
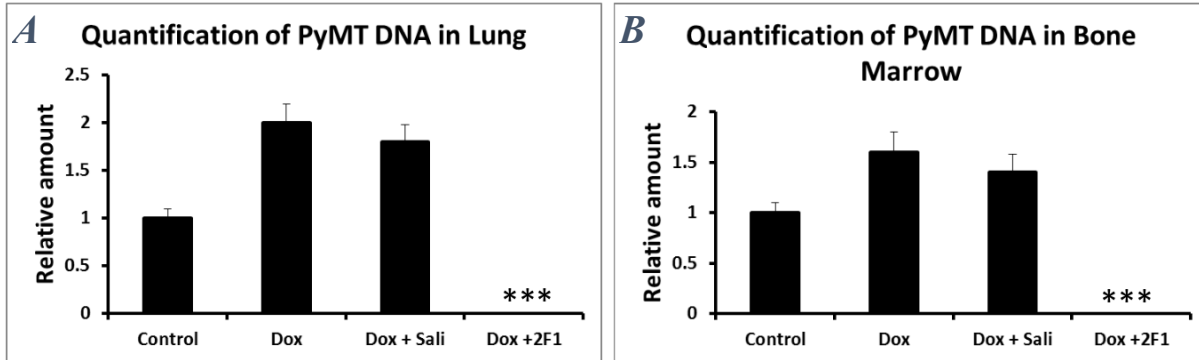
Fig 3: Inhibition of MET-1 lung and bone marrow metastasis by Doxorubicin, Salinomycin, and Mab 2F1 Met-1 Tumors in FvB mice were injected with Dox (2mg/Kg), Salinomycin (5mg/Kg), and 2F1 (5mg/Kg) for 5 weeks after which the lung and bone marrow was extracted, and qRT-PCR performed for PyMT gene. (A) Lung Tissue: relative amount of Dox (2), Dox+Sali (1.8), and Dox+2F1(undetectable) to control (1) was analyzed for statistical significance. (B) Bone Marrow: relative amount of Dox (1.7), Dox+Sali (1.5), and Dox+2F1(undetectable) to control (1) was analyzed for statistical significance. N=5, *= p < 0.05, ***= p < 0.001

Figure 3 shows a significant reduction in Met-1 metastasis in both lung and bone marrow tissue by Dox+2F1 treatment. It was observed that Dox+2F1 treated group has significantly less PyMT gene expression (p= 0.00052) in lung tissue and bone marrow (p= 0.00017) compared to control and compared to Dox and Dox+Sali individually. Interestingly, Dox and Dox+Sali groups relative amount was determined to be not significantly different than the controls in both lung and bone marrow analysis (p > 0.05 for all). By this observation, we can conclude that 2F1 significantly reduces lung and bone marrow metastasis in FVB mice and is more effective than both Dox and Dox+Sali treatments.

Discussion

The experimental plan for this study was designed with the goal of furthering our understanding of LRP6 function in breast cancer metastasis and tumor growth, analyzing the potential of 2F1 as a targeted therapy to treat metastatic breast cancer, and gaining insight into the role of the Wnt signaling pathway in breast cancer stem cell (BCSC) formation. In this study, the hypothesis that 2F1 would perform more effectively to reduce mammary cancer tumor growth and metastasis in-vivo than both standard chemotherapy treatment (Doxorubicin) and an approved small molecule Wnt inhibitor therapy (Salinomycin) was tested and supported. Treatment of MET-1 tumors in-vivo with Dox+2F1 provided significant and promising results in comparison with Dox, Dox+Sali, and Control trial groups. 2F1 tumor reduction ability was significantly more effective than that of Dox+Sali, Dox, and control (p <.005, Figure 2). Mice in the 2F1 treatment group had the lowest average tumor size by the end of the 5-week study as well as the lowest prevalence of necrosis. Necrosis is an indicator of advanced tumor formation and is often associated with poor prognosis of cancer patients (Liu, 2020). Thus, the lower prevalence of necrosis is an additional indicator of effective treatment by 2F1 in the tumor growth model.

Furthermore, 2F1 was observed as a successful metastatic inhibitor. PyMT genetic expression was significantly lower (p< 0.001) in Dox+2F1 treatment group when compared to the other trials. This indicates 2F1's metastatic prevention surpasses both conventional chemotherapy and the biological targeted therapy Salinomycin. This also shows the 5mg/kg 2F1 dosage used to be effective in providing adequate amount of monoclonal antibody to silence LRP6 receptors on BCSCs while maintaining normal LRP6 function in healthy cells.

Unexpectedly, Dox and Dox+Sali treatment was found to be ineffective in both tumor reduction and metastatic prevention. At the administered dosage, Dox (2mg/kg) and Dox+Sali (5mg/kg) treatment data were both concluded to be not significantly different than that of the control. These findings conflict both with the literature that cites chemotherapy to be more effective than no treatment and the literature that supports Salinomycin as a LRP6 silencer. These findings are surprising and could indicate an issue with the FVB model used and/or signify an internal issue with the study. However, these results are similar to those of our lab's peers at Einstein Medical School and we believe that the relationship between the increased metastatic appearance in Dox+Sali groups should be further explored.

A potential explanation for the discrepancy of Dox and Salinomycin behavior from the foundational literature is the low dosage that was selected. A 2mg/kg dosage of Dox was selected based on a range determined Wayne Aston as he studied the maximum tolerant dose of chemotherapy for mice— he generated a range of tolerance between 2mg/kg and 12mg/kg (Aston, 2017). The 2mg/kg was the lowest dosage found to be effective and was designated specifically to ensure maximum survivability and reduce side effects from the chemotherapy. It is likely that a larger dosage is needed to ensure effectiveness.

For Salinomycin, the 5mg/kg dosage appears to be too low to effectively operate in-vivo. As a small molecule, Salinomycin has low water-solubility, high pharmacokinetics, and low circulation half-life that complicate its bioavailability in-vivo (Li, 2019). Even at a higher dosage, delivery of Salinomycin more frequently than once a week may be necessary for in-vivo

viability. In comparison, 2F1 naturally has a high bioavailability and a longer circulation half-life as a monoclonal antibody (Ovacik, 2018). Circulation half-life and bioavailability is an important aspect of a potential therapeutic agent and the smaller amount of 2F1 necessary to effectively silence LRP6 provides a concrete clinical advantage over Salinomycin.

Importantly, this research introduces the monoclonal antibody 2F1 as a promising antitumor and antimetastatic treatment and lays the foundation for its utilization as a breast cancer targeted therapy for patients with tumor overexpression of LRP6. To further establish the promise of 2F1, this groundwork should be expanded upon through a number of future extensions. Although data gathered in this study is reliably correlated to performance in human breast cancer, the PyMT FVB mouse model utilizes mouse mammary cancer that is not identical physiologically to human cancer. Thus, a study utilizing a human breast cancer cell line in an immune compromised SCID mouse model would further concretize the effectiveness of 2F1 and better signify its potential performance in clinical trials. Another shortcoming of this experiment was that the tumors remained present during treatment. Realistic treatment of breast cancer involves removal of the tumor mass and then subsequent targeted therapy and the presence of the tumor may have exacerbated some metastatic qualities. A study involving surgical removal of the tumor before therapy administration may provide more translational results. Certainly, further energy should also be dedicated to determining more accurate in-vivo dosage levels for Doxorubicin and Salinomycin.

Possible error within this study may have occurred due to multiple factors. For one, the sample sizes for each treatment group (n =5) are the minimum for statistical analysis and would be more reliable if each trial contained more specimen. Additionally, error may have occurred during the caliper reading of tumor size. Necrosis may have had a significant impact on tumor size and may have positively skewed the data recorded. Analyzing tumor size is inherently complicated due to the cocktail of environmental and genetic factors that influence tumor formation. There may be overlooked factors and influences that impact MET-1 tumor formation that need to be further understood. However, protocols utilized in this study were designed to combat these potential sources of errors and error did not significantly impact the results. The deductions draw from this study are reliable and drawn with confidence.

In conclusion, the results from this study suggest that 2F1 and, more generally LRP6 silencing with monoclonal antibody therapy at the cell surface, can be potential therapeutic targets in breast cancer treatment. This investigation establishes the ability of 2F1 to bind to the LRP6 receptor and silence the frizzle/canonical Wnt signaling pathway through intraperitoneal injection in-vivo. The 2F1 data recorded corroborates the proposed BCSC/Wnt theory of metastasis and implicates LRP6 and cell surface Wnt signaling as a major player as a facilitator of BCSC self-renewal and stemness. Supporting the role of cancer stem cells and the Wnt pathway in causing metastasis within breast cancer, these conclusions may indicate the role of cancer stem cells as a fundamental aspect of cancer progression inherent in all cancer cell lines. Moreover, this study demonstrates 2F1 has potential to be an ideal LRP6 targeted therapy because of its ability to sufficiently reduce Wnt signaling to inhibit metastasis without contributing significant toxicity. Further resources should be allocated to study 2F1 and potentially push it closer to clinical trials.

Sources

1. Goswami, S., et al., Breast cancer cells isolated by chemotaxis from primary tumors show increased survival and resistance to chemotherapy. Cancer Res, 2004. 64(21): p. 7664-7.

2. Roussos, E.T., et al., Mena invasive (Mena (INV)) and Mena11a isoforms play distinct roles in breast cancer cell cohesion and association with TMEM. Clin Exp Metastasis, 2011. 28(6): p. 515-27.

3. Robinson, B.D., et al., Tumor microenvironment of metastasis in human breast carcinoma: a potential prognostic marker linked to hematogenous dissemination. Clin Cancer Res, 2009. 15(7): p. 2433-41.

4. Leong Tam W. and Weinberg RA., The epigenetics of epithelial-mesenchymal plasticity in cancer. Nature Med, 2013. 19(11): 1438-1449.

5. Al-Hajj, M., Wicha, M.S., Benito-Hernandez, A., Morrison, S.J. & Clarke, M.F. Prospective identification of tumorigenic breast cancer cells. Proc Natl Acad Sci USA 100, 3983–8 (2003).

6. Liu, H. et al. Cancer stem cells from human breast tumors are involved in spontaneous metastases in orthotopic mouse models. Proc Natl Acad Sci USA 107, 18115–20 (2010).

7. Nguyen LV, Vanner R, Dirks P, Eaves CJ. Cancer stem cells: an evolving concept. Nat Rev Cancer 2012; 12: 133–143.

8. Desheng Lu1,2, Michael Y. Choi1, Jian Yu1, Januario E. Castro, Thomas J. Kipps, and Dennis A. Carson. Salinomycin inhibits Wnt signaling and selectively induces apoptosis in chronic lymphocytic leukemia cells. PNAS | August 9, 2011 | vol. 108 | no. 32 | 13253–13257.

9. Gupta PB, et al. (2009) Identification of selective inhibitors of cancer stem cells by high-throughput screening. Cell 138:645–659.

10. Sheridan, C. et al. CD44+/CD24− breast cancer cells exhibit enhanced invasive properties: an early step necessary for metastasis. Breast Cancer Res 8, R59 (2006).

11. Marco A. Velasco-Velázquez,Vladimir M. Popov, Michael P. Lisanti, and Richard G. Pestell. The Role of Breast Cancer Stem Cells in Metastasis and Therapeutic Implications. The American Journal of Pathology, Vol. 179, No. 1, July 2011

12. Jeanine Pignatelli, Sumanta Goswami, Joan G. Jones, Thomas E. Rohan, Evan Pieri, Xiaoming Chen, Esther Adler, Dianne Cox, Sara Maleki, Anne Bresnick, Frank B. Gertler, John S. Condeelis, and Maja H. Oktay. Invasive breast carcinoma cells from patients exhibit MenaINV- and macrophage-dependent transendothelial migration. Sci Signal. ; 7(353)

13. Liu S., etal., Hedgehog signaling and Bmi-1 regulate self-renewal of normal and malignant human mammary stem cells. Cancer Res., 2006. 66 (12): 6063–71

14. Brennan A.K., etal.., Combining Notch inhibition with current therapies for breast cancer treatment .Ther Adv Med Oncol ,2013. 5(1) 17–24.

15. Bankers J.L, et.al.,Interleukin-1 signal transduction. Life Sciences, 1996. 59 (2): 61–83

16. Dinarello C.A. Induction of interleukin-1 and interleukin-1 receptor antagonist. Seminars in Oncology, 1997. 24

17. Liu, H. et al. Cancer stem cells from human breast tumors are involved in spontaneous metastases in orthotopic mouse models.Proc Natl Acad Sci USA, 2010. 107, 18115–20.

18. Zhong .Li. CD133 a stem cell biomarker and beyond. Exp Hematol Oncol, 2013. 2: 17. :

19. Kinzler K.W. etal., Identification of an amplified, highly expressed gene in a human glioma. Science, 1987. 236 (4797): 70–3

20. Soyoung I.m. etal.. Hedgehog Related Protein Expression in Breast Cancer: Gli-2 Is Associated with Poor Overall Survival. The Korean Journal of Pathology 2013; 47: 116-

21. Corti S, Locatelli F, Papadimitriou D, Donadoni C, Salani S, Del Bo R, Strazzer S, Bresolin N, Comi GP: Identification of a primitive brainderived neural stem cell population based on aldehyde dehydrogenase activity. Stem Cells 2006, 24:975–985

22. Fuchs, E.; Tumbar, T.; Guasch, G. Socializing with the neighbors: Stem cells and their niche. Cell 2004, 116, 769–778.

23. Ye, J.;Wu, D.;Wu, P.; Chen, Z.; Huang, J. The cancer stem cell niche: Cross talk between cancer stem cells and their microenvironment. Tumour. Biol. 2014, 35, 3945–3951.

24. King TD, Suto MJ, Li YH. The Wnt/b-Catenin signaling pathway: a potential therapeutic target in the treatment of triple negative breast cancer. J Cell Biochem 2012; 113: 13–18.

25. Polakis P. The many ways of Wnt in cancer. Curr Opin Genet Dev 2007; 17: 45–51.

26. Lu D, Choi MY, Yu J, Castro JE, Kipps TJ, Carson DA et al. Salinomycin inhibits Wnt signaling and selectively induces apoptosis in chronic lymphocytic leukemia cells. PNAS 2011; 108: 13253–13257.

27. Liu CC1, Prior J, Piwnica-Worms D and Bu G. LRP6 overexpression defines a class of breast cancer subtype and is a target for therapy. Proc Natl Acad Sci U S A. 2010 Mar 16;107(11):5136-41.

28. Hu Y1, Chen Y, Lin M, Lee K, Mott RA and Ma JX. Pathogenic role of the Wnt signaling pathway activation in laser-induced choroidal neovascularization. Invest Ophthalmol Vis Sci. 2013 Jan 7;54(1):141-54.

29. Eaves, C.J. & Humphries, R.K. Acute myeloid leukemia and the Wnt pathway. N Engl J Med 362, 2326–7 (2010).

30. Gyu-Beom Jang, Ji-Young Kim Sung-Dae Cho, Ki-Soo Park, Ji-Youn Jung, Hwa-Yong Lee, In-Sun Hong & Jeong-Seok Nam. Blockade of Wnt/β-catenin signaling suppresses breast cancer metastasis by inhibiting CSC-like phenotype. Scientific Reports | 5:12465. 2015

31. Liu, Anne Schott1, Dan Hayes1, Daniel Birnbaum3, Max S. Wicha1, and Gabriela Dontu1. ALDH11 is a marker of normal and malignant human mammary stem cells and a predictor of poor clinical outcome. Cell Stem Cell. 2007 November 15; 1(5): 555–567.

32. Li J, Zhai L, Xue J, Zhang H, Xie F, Gao J. Effects of D-α-tocopherol polyethylene glycol succinate-emulsified poly(lactic-co-glycolic acid) nanoparticles on the absorption,

pharmacokinetics, and pharmacodynamics of salinomycin sodium. Anticancer Drugs. 2019 Jan;30(1):72-80. doi: 10.1097/CAD.0000000000000695. PMID: 30239423.

33. Yin, P., Wang, W., Zhang, Z., Bai, Y., Gao, J., & Zhao, C. (2018). Wnt signaling in human and mouse breast cancer: Focusing on Wnt ligands, receptors and antagonists. *Cancer science*, *109*(11), 3368–3375. https://doi.org/10.1111/cas.13771

34. Plaks, V., Kong, N., & Werb, Z. (2015). The cancer stem cell niche: how essential is the niche in regulating stemness of tumor cells?. *Cell stem cell*, *16*(3), 225–238. https://doi.org/10.1016/j.stem.2015.02.015

35. Xu, X., Zhang, M., Xu, F. *et al.* Wnt signaling in breast cancer: biological mechanisms, challenges and opportunities. *Mol Cancer* **19,** 165 (2020). https://doi.org/10.1186/s12943-020-01276-5

36. Reya T, Clevers H. Wnt signalling in stem cells and cancer. Nature. 2005 Apr 14;434(7035):843-50. doi: 10.1038/nature03319. PMID: 15829953.

37. Vermeulen, L. (2010). Wnt Signaling in Cancer Stem Cell Biology. *Cancers*, *8*(7), 60. https://doi.org/10.3390/cancers8070060

38. Su YJ, Chang YW, Lin WH, Liang CL, Lee JL. An aberrant nuclear localization of E-cadherin is a potent inhibitor of Wnt/β-catenin-elicited promotion of the cancer stem cell phenotype. Oncogenesis. 2015 Jun 15;4(6):e157. doi: 10.1038/oncsis.2015.17. PMID: 26075748; PMCID: PMC4491612.

39. Hoffmeyer K, Raggioli A, Rudloff S, Anton R, Hierholzer A, Del Valle I, Hein K, Vogt R, Kemler R Science. 2012 Jun 22; 336(6088):1549-54.

40. Komiya, Y., & Habas, R. (2008). Wnt signal transduction pathways. *Organogenesis*, *4*(2), 68–75. https://doi.org/10.4161/org.4.2.5851

41. Ma J, Lu W, Chen D, Xu B, Li Y. Role of Wnt Co-Receptor LRP6 in Triple Negative Breast Cancer Cell Migration and Invasion. J Cell Biochem. 2017 Sep;118(9):2968-2976. doi: 10.1002/jcb.25956. Epub 2017 May 30. PMID: 28247948.

42. Liu CC, Prior J, Piwnica-Worms D, Bu G. LRP6 overexpression defines a class of breast cancer subtype and is a target for therapy. Proc Natl Acad Sci U S A. 2010 Mar 16;107(11):5136-41. doi: 10.1073/pnas.0911220107. Epub 2010 Mar 1. PMID: 20194742; PMCID: PMC2841938.

43. Schmitt M, Metzger M, Gradl D, Davidson G, Orian-Rousseau V. CD44 functions in Wnt signaling by regulating LRP6 localization and activation. Cell Death Differ. 2015 Apr;22(4):677-89. doi: 10.1038/cdd.2014.156. Epub 2014 Oct 10. PMID: 25301071; PMCID: PMC4356338.

44. Lu D, Choi MY, Yu J, Castro JE, Kipps TJ, Carson DA. Salinomycin inhibits Wnt signaling and selectively induces apoptosis in chronic lymphocytic leukemia cells. Proc Natl Acad Sci U S A. 2011 Aug 9;108(32):13253-7. doi: 10.1073/pnas.1110431108. Epub 2011 Jul 25. PMID: 21788521; PMCID: PMC3156152.

45. Lee, Kyungwon & hu, Yang & Ding, Lexi & Chen, Ying & Yusuke, Takahashi & Mott, Robert. (2012). Therapeutic Potential of a Monoclonal Antibody Blocking the Wnt

Pathway in Diabetic Retinopathy. Diabetes. 61. 2948-57. 10.2337/db11-0300. Altundag K, Esteva FJ, Arun B. Monoclonal antibody-based targeted therapy in breast cancer. Curr Med Chem Anticancer Agents. 2005 Mar;5(2):99-106. doi: 10.2174/1568011053174846. PMID: 15777217.

46. Lee K, Hu Y, Ding L, Chen Y, Takahashi Y, Mott R, Ma JX. Therapeutic potential of a monoclonal antibody blocking the Wnt pathway in diabetic retinopathy. Diabetes. 2012 Nov;61(11):2948-57. doi: 10.2337/db11-0300. Epub 2012 Aug 13. PMID: 22891217; PMCID: PMC3478529.

47. Christenson JL, Butterfield KT, Spoelstra NS, Norris JD, Josan JS, Pollock JA, McDonnell DP, Katzenellenbogen BS, Katzenellenbogen JA, Richer JK. MMTV-PyMT and Derived Met-1 Mouse Mammary Tumor Cells as Models for Studying the Role of the Androgen Receptor in Triple-Negative Breast Cancer Progression. Horm Cancer. 2017 Apr;8(2):69-77. doi: 10.1007/s12672-017-0285-6. Epub 2017 Feb 13. PMID: 28194662; PMCID: PMC5407486.

48. Simmons, J. K., Hildreth, B. E., 3rd, Supsavhad, W., Elshafae, S. M., Hassan, B. B., Dirksen, W. P., Toribio, R. E., & Rosol, T. J. (2015). Animal Models of Bone Metastasis. *Veterinarypathology*, *52*(5),827–841.
https://doi.org/10.1177/0300985815586223

49. ThermoFisher, William W. Wilfinger, Karol Mackey, and Piotr Chomczynski, Effect of pH and Ionic Strength on the Spectrophotometric Assessment of Nucleic Acid Purity: BioTechniques 22:474-481 (March 1997.)

50. Morton, J., & Snider, T. A. (2017). Guidelines for collection and processing of lungs from aged mice for histological studies. *Pathobiology of aging & age related diseases*, *7*(1), 1313676. https://doi.org/10.1080/20010001.2017.1313676

51. Ovacik, M., & Lin, K. (2018). Tutorial on Monoclonal Antibody Pharmacokinetics and Its Considerations in Early Development. *Clinical and translational science*, *11*(6), 540–552. https://doi.org/10.1111/cts.12567

52. Enot, D. P., Vacchelli, E., Jacquelot, N., Zitvogel, L., & Kroemer, G. (2018). TumGrowth: An open-access web tool for the statistical analysis of tumor growth curves. *Oncoimmunology*, *7*(9), https://doi.org/10.1080/2162402X.2018.1462431

Acknowledgements

There are many people I would like to thank who helped me on this journey and without whom this project would not have been possible. First and foremost, I would like to thank my mentor Dr. Goswami. Without your guidance and tutelage over these past four years, I would not have the appreciation for the wonders of biomedical research that I have today. Your patience and faith in me have helped me mature not only inside the lab, but also outside it and has sharpened me into the person that I am proud to be today. I would also like to thank Dr. Gargi Bandyopadhyaya, who has worked with me in the Goswami Lab over these past four years. Your dedication our labs research is inspiring, and I thank you for kindly making the time for me and taking me under your wing. Additionally, I am grateful for the amazing faculty at Yeshiva College, who have educated me and supported me over these past four years. Their guidance and commitment to the highest level of learning provided a foundation with which I will build for the rest of my life. Lastly, I would also like to thank the Jay and Jeannie Schottenstein Honors Program of Yeshiva College for providing me with both support for this project as well as unbelievable educational opportunities throughout my time as an undergraduate. Sincerely, Thank You.